

Learning to Importance Sample in Primary Sample Space

QUAN ZHENG, University of Maryland, College Park

MATTHIAS ZWICKER, University of Maryland, College Park



Fig. 1. Our method learns to importance in primary sample space. While our approach is independent of specific light transport effects, we apply it here to direct and one bounce indirect illumination. This scene has 27 light sources, and we achieve a significant variance reduction over uniformly sampling the lights.

Importance sampling is one of the most widely used variance reduction strategies in Monte Carlo rendering. In this paper, we propose a novel importance sampling technique that uses a neural network to learn how to sample from a desired density represented by a set of samples. Our approach considers an existing Monte Carlo rendering algorithm as a black box. During a scene-dependent training phase, we learn to generate samples with a desired density in the primary sample space of the rendering algorithm using maximum likelihood estimation. We leverage a recent neural network architecture that was designed to represent real-valued non-volume preserving (“Real NVP”) transformations in high dimensional spaces. We use Real NVP to non-linearly warp primary sample space and obtain desired densities. In addition, Real NVP efficiently computes the determinant of the Jacobian of the warp, which is required to implement the change of integration variables implied by the warp. A main advantage of our approach is that it is agnostic of underlying light transport effects, and can be combined with many existing rendering techniques by treating them as a black box. We show that our approach leads to effective variance reduction in several practical scenarios.

CCS Concepts: • **Computing methodologies** → **Rendering; Ray tracing**;

Additional Key Words and Phrases: ray tracing, global illumination, importance sampling, neural networks

Authors’ addresses: Quan Zheng, University of Maryland, College Park, quan.zheng@outlook.com; Matthias Zwicker, University of Maryland, College Park, zwicker@cs.umd.edu.

Permission to make digital or hard copies of all or part of this work for personal or classroom use is granted without fee provided that copies are not made or distributed for profit or commercial advantage and that copies bear this notice and the full citation on the first page. Copyrights for components of this work owned by others than ACM must be honored. Abstracting with credit is permitted. To copy otherwise, or republish, to post on servers or to redistribute to lists, requires prior specific permission and/or a fee. Request permissions from permissions@acm.org.

© 2018 Association for Computing Machinery.

XXXX-XXXX/2018/6-ART1 \$15.00

<https://doi.org/10.1145/nnnnnnn.nnnnnnn>

ACM Reference Format:

Quan Zheng and Matthias Zwicker. 2018. Learning to Importance Sample in Primary Sample Space. 1, 1, Article 1 (June 2018), 11 pages. <https://doi.org/10.1145/nnnnnnn.nnnnnnn>

1 INTRODUCTION

Importance sampling has been recognized as a key technique for variance reduction right from the inception of Monte Carlo rendering algorithms [13]. Today, importance sampling of BRDFs, environment maps, direct illumination from many light sources, or visibility are standard features in Monte Carlo path tracing systems. A number of advanced techniques have also been developed to jointly importance sample several of these factors. Many of these approaches rely on an analytical analysis of scene properties, such as the surface appearance models and BRDFs used in the scenes.

In contrast, we propose a technique that treats an existing Monte Carlo renderer as a black box and learns how to importance sample entire paths in primary sample space (Figure 1). Our approach first acquires a set of training samples for a given scene using the existing renderer. Based on these samples, we learn to generate a desired scene-dependent target density in the primary sample space (PSS) of that renderer. In the subsequent rendering step, instead of feeding the renderer with uniform PSS samples, we provide samples drawn from the learned target density. By specifying a suitable target density, we achieve effective variance reduction compared to using the existing renderer with the usual uniform primary sample space.

The key component of our approach is a recent neural network architecture that was designed to represent real-valued non-volume preserving (“Real NVP”) transformations in high dimensional spaces. This approach learns a one-to-one, non-linear warp between two high-dimensional spaces. In addition, the computation of the warp

is structured such that the forward warp, its inverse, and the determinant of its Jacobian can all be computed effectively. We leverage these properties to learn a warp from a uniform to a desired non-uniform target density in primary sample space. The advantages of our approach are that it treats a renderer as a black box and is agnostic to specific light transport effects, hence it can be combined with many existing algorithms.

Conceptually, our approach has similarities to several previous strategies. Primary sample space Metropolis (PSS-MLT) sampling can also importance sample any desired target density by operating in primary sample space while treating an existing renderer as a black box [16], similar to our approach. PSS-MLT can be inefficient, however, because it often needs to reject many proposed paths to achieve the desired density. In contrast, our approach never rejects samples during rendering. Several previous techniques acquire a set of initial samples to build up data structures that approximate the desired density, and then can be used to perform importance sampling during subsequent rendering passes. The advantage of our approach is that we treat the renderer as a black box, and we do not need to implement additional data structures such as octrees, spatial samplings of the scene, or explicit density models. Instead, the information learned from an initial set of samples is captured by the Real NVP neural network. In summary, the main contributions of this paper are:

- A novel formulation of importance sampling of entire light paths as a non-linear warp in primary sample space.
- A novel technique to learn the primary sample space warp using a suitable neural network architecture.
- A demonstration that this approach can effectively reduce variance of Monte Carlo path tracers in several scenarios.

2 RELATED WORK

2.1 Importance sampling in Monte Carlo Rendering

Already when introducing the rendering equation, Kajiya [13] discussed importance sampling as a technique to reduce variance in Monte Carlo rendering. Importance sampling aims to obtain samples with a probability density that is proportional to a desired target density function, and by designing target densities similar to the integrand, variance can be reduced. In Monte Carlo path tracing, the target density function can be defined either as a product of local densities in an incremental manner, or directly as a density in global path space. Accordingly, two categories of importance sampling techniques have been studied in past decades.

Incremental sampling. When light paths are constructed in an incremental way, it is natural to perform importance sampling locally in each step. For example, BRDF and light sampling techniques construct a path segment by separately mimicking the local distribution of cosine weighted BRDF and incident illumination, respectively. To further reduce the estimator’s variance, Veach and Guibas [24] introduced multiple importance sampling to combine the advantages of individual path sampling techniques. We refer to standard texts for an overview of the extensive literature [21]. In general, importance sampling techniques can be categorized into two broad groups: “a priori” methods that construct target densities and sampling techniques using analytical approximations of the

integrand (for example, Heitz and d’Eon [11] among many others), and “a posteriori” methods that fit target densities based on empirically acquired samples of the integrand [19, 27]. The technique by Clarberg [5] is an a priori method that performs importance sampling of products of environment maps, BRDFs, and visibility by representing them using wavelets. They achieve importance sampling by evaluating wavelet products on the fly and constructing a hierarchical warp accordingly, which has some similarities to our warp-based importance sampling. Our approach, however, operates in an a posteriori manner and it does not rely on a specific representation of the integrand, such as using wavelet products. Our approach is also more general and can be applied to any light transport effect. Recently, a Bayesian method has been proposed to sample direct illumination that can be considered a combination of a priori and a posteriori strategies [26]. Our approach considers entire light paths instead of performing incremental sampling, and is not limited to direct illumination sampling.

Global sampling. Instead of importance sampling individual path segments, Metropolis light transport [25] treats a complete path as a single sample in a global path space that is also used to define the target density. A new path is sampled from a Markov process by mutating an existing path according to a scalar contribution function. Various parameterizations of path space have been proposed to efficiently explore it using Markov chain methods [12, 15, 16, 18], and techniques have been proposed to combine different parameterizations to even further improve the sampling process [3, 9, 20].

Our approach is similar to global path sampling techniques since we also importance sample entire paths. In particular, we also sample paths in primary sample space as proposed by Kelemen et al. [16], which is simply a multi-dimensional unit cube. As in Kelemen’s approach, we also build on existing path construction techniques that map primary sample space parameters into geometric paths, and that we treat as a black box. In contrast, our approach does not rely on Markov chain sampling, however. Instead, we obtain a non-linear, one-to-one mapping of primary sample space onto itself that produces the desired target density.

2.2 Deep Learning to Sample Complex Data Distributions

Recently, various neural network architectures have been proposed to learn generative models of high-dimensional data, such as images and videos. A generative model learns to transform random samples from a latent space into samples of some observable data, for example images, such that the distribution of the generated data matches the distribution of an observed set of data samples. Some of the most successful techniques include generative adversarial networks (GANs) [8] and variational autoencoders (VAEs) [17]. Our idea is to use such a learned mapping from a latent to a data space to perform importance sampling of entire light paths. A key requirement for this is that we need to be able to efficiently compute the Jacobian of this mapping, such that we can use it to perform a change of integration variables. However, the computation of the Jacobian involved in deep neural network is costly in techniques such as GANs or VAEs. Instead, we leverage a recent neural network architecture

called “Real NVP” [6] that was specifically designed as an invertible mapping whose Jacobian can be computed easily.

2.3 Deep Learning in Monte Carlo Rendering

Deep learning has been successfully applied to denoise Monte Carlo rendering results [2, 4], and such techniques are commonly used in production rendering today. Our approach is orthogonal to these techniques and can be combined with any state of the art denoiser. Neural networks have also been used as a regression architecture to interpolate radiance values from sparse samples [14, 22]. These methods, however, do not converge to ground truth solutions, since they rely on directly predicting radiance based on a model learned from a limited amount of data. In contrast, we learn how to sample, and we compute accurate sampling densities that can be used to perform unbiased importance sampling. While we do not have a theoretical proof that our approach reduces variance, we demonstrate significant variance reduction in several practical scenarios.

3 BACKGROUND

The path integral formulation [25] of the rendering equation [13] expresses the value I_j of each pixel j as an integral over the space of all light paths,

$$I_j = \int_{\Omega} f_j(x) d\mu(x), \quad (1)$$

where x is a light path, $d\mu$ is a measure on the space of paths, and f_j is the measurement contribution function. In addition, Ω is the space of all light paths, consisting of the union of light paths of all lengths k , $\Omega = \cup_k \Omega_k$.

An important observation is that there are many ways to parameterize light paths, and each parameterization has its own measure $d\mu$. Considering only light paths of a certain length k , however, it is always possible to define a mapping Φ_k from a canonical parameterization over the $2(k+1)$ -dimensional unit cube¹ to Ω_k , that is, $\Phi_k : [0, 1]^{2(k+1)} \rightarrow \Omega_k$. This is also called primary sample space [16], and indeed each Monte Carlo rendering algorithm implicitly evaluates Φ_k when constructing light paths. Using Φ_k to perform a change of integration variables, we can rewrite the path integral formulation as

$$I_{j,k} = \int_{\Omega_k} f_j(x) d\mu(x) = \int_{[0,1]^{2(k+1)}} f_j(\Phi_k(y)) \left| \frac{\partial \Phi_k(y)}{\partial y} \right| dy, \quad (2)$$

where $I_{j,k}$ denotes the contribution of all paths of length k to pixel j , $y \in [0, 1]^{2(k+1)}$, and the notation $|\cdot|$ is shorthand for the determinant of the Jacobian matrix. Figure 2(a) illustrates the notation in Equation 2.

In this view, incremental importance sampling techniques discussed in Section 2.1 imply certain mappings Φ_k from primary sample space to geometric paths, and the effect of importance sampling is absorbed in the mapping Φ_k . Usually, the integral in Equation 2 is estimated using uniform sampling in primary sample space,

¹This assumes that path vertices are on surfaces, and each of them is parameterized using two numbers. Depending on the details of the renderer, however, more parameters may be involved in practice, for example to select BRDF components.

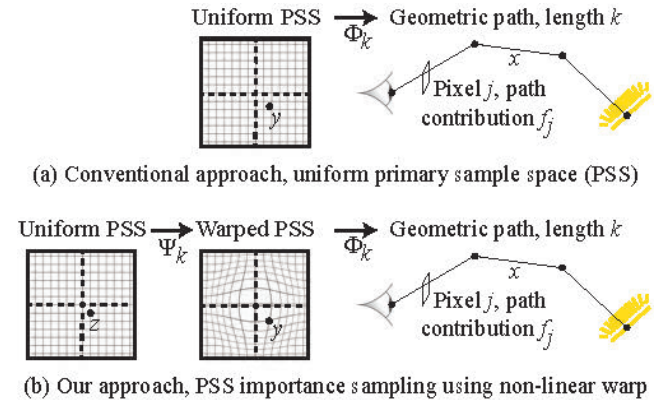


Fig. 2. Comparison of the conventional approach and ours: (a) Usually, primary sample space (PSS) is sampled uniformly. Each point y in primary sample space (PSS) of dimension $2(k+1)$ corresponds to a geometric path x of length k via a mapping Φ_k . Conventional importance sampling is accounted for by the determinant of the Jacobian of Φ_k . (b) Our approach introduces a non-linear warp Ψ_k in primary sample space to further reduce variance, and we learn this mapping using a neural network.

$$I_{j,k} \approx \frac{1}{N} \sum_{i=1}^N \frac{f_j(\Phi_k(y_i))}{\left| \frac{\partial \Phi_k(y_i)}{\partial y_i} \right|^{-1}}, \quad (3)$$

where the $y_i \in [0, 1]^{2(k+1)}$ are uniform random samples. The goal of importance sampling is to construct suitable mappings Φ_k with determinants that are inversely proportional to f_j as much as possible², which will reduce variance of the estimate in Equation 3. Incremental importance sampling approaches, however, rely only on local information about f_j , hence they are unable to account for non-local effects.

4 PRIMARY SAMPLE SPACE (PSS) WARPING

As illustrated in Figure 2(b), the key idea of our approach is to introduce an additional mapping of primary sample space onto itself, acting as a non-uniform warp that leads to a non-uniform PSS density. We design this density to further reduce the variance of an existing renderer that evaluates Equation 3, which we treat as a black box. We learn the warp in a scene-dependent training phase, and then use it to draw as many samples for rendering as desired.

In the following, we describe how we construct the warp in the training phase. We start by introducing the details of our problem statement in Section 4.1. We then explain in Section 4.2 how we achieve the objective of the PSS warp using an “a posteriori” approach. This involves first drawing a number of samples from Equation 3 and resampling them to obtain the desired target density. Then we use a maximum likelihood estimation of the warp to match the target density. In Section 4.3 we describe how we represent the warp in practice using the Real NVP architecture and solve the maximum likelihood estimation via gradient descent. We describe the

²The determinant of the Jacobian is the inverse of the corresponding sampling density.

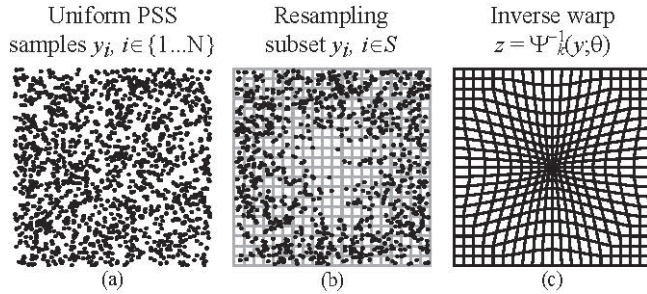


Fig. 3. We illustrate how we learn the inverse warp $\Psi_k^{-1}(y; \theta)$ to match a target density. (a) We first obtain uniform samples in PSS. (b) We resample them to obtain samples from the target density. (c) The inverse warp $\Psi_k^{-1}(y; \theta)$ is computed to maximize the likelihood of the target samples under the warp.

details of the neural networks involved in Real NVP in Section 4.4, and describe how we use the warp during rendering in Section 4.5.

4.1 Problem Formulation

Let us denote the PSS warp that we will learn as

$$\Psi_k : [0, 1]^{2(k+1)} \rightarrow [0, 1]^{2(k+1)}. \quad (4)$$

Assuming this is bijective and differentiable, we can use it to introduce an other change of integration variables $y = \Psi_k(z)$ in Equation 2,

$$I_{j,k} = \int_{[0,1]^{2(k+1)}} f_j(\Phi_k(\Psi_k(z))) \left| \frac{\partial \Psi_k(z)}{\partial z} \right| \left| \frac{\partial \Phi_k(\Psi_k(z))}{\partial \Psi_k(z)} \right| dz. \quad (5)$$

This leads to the Monte Carlo estimate

$$I_{j,k} \approx \frac{1}{N} \sum_{i=1}^N \frac{f_j(\Phi_k(\Psi_k(z_i)))}{\left| \frac{\partial \Psi_k(z_i)}{\partial z_i} \right|^{-1} \left| \frac{\partial \Phi_k(\Psi_k(z_i))}{\partial \Psi_k(z_i)} \right|^{-1}}, \quad (6)$$

where the $z_i \in [0, 1]^{2(k+1)}$ are uniform random samples. To reduce variance of this, we want to design Ψ_k such that the integrand in Equation 5 is as close as possible to a constant. Note that the determinant of the Jacobian of our primary sample space warp, $|\partial \Psi_k(z)/\partial z|$ is the inverse of the desired non-uniform sampling density in a warped primary sample space, which serves as input to the black-box renderer.

Practical Simplifications. Our description so far implies that we would need to learn a mapping Ψ_k for each pixel. This is impractical, however, and we will make the simplification to replace the measurement contribution function f_j by the path throughput f , which is related to the measurement contribution by omitting the pixel filter (also called the importance function). In addition, we only learn mappings for certain path lengths, and leave the sampling of other paths unchanged. Removing these current restrictions is subject of future work.

4.2 Maximum Likelihood Estimation of the PSS Warp

As illustrated in Figure 3, we follow an ‘‘a posteriori’’ approach to learn the PSS warp by first drawing a set of samples from a desired

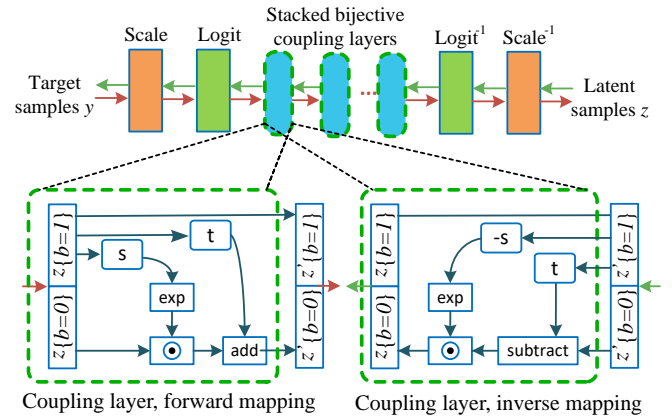


Fig. 4. Computational structure of our neural importance sampling model based on Real NVP. The core element of this architecture consists of a set of stacked, invertible coupling layers. The functions s and t are implemented using neural networks as shown in Figure 5, and stacking several coupling layers makes it possible to represent complex, bijective mappings.

target density in primary sample space. Then we estimate the warp under a maximum likelihood objective for these observed samples.

Sampling the Target Density. As mentioned above, in this paper we use the path throughput f to define our target density as

$$p_Y(y) = \frac{f(\Phi_k(y))}{\left| \frac{\partial \Phi_k(y)}{\partial y} \right|^{-1}}, \quad (7)$$

although any other target density could be used. We obtain a number of samples $y \sim p_Y$ from this distribution using a resampling process as proposed by Talbot et al. [23]. This involves rendering a set T of N samples using a uniform PSS density, as usual, and storing the PSS parameters and path throughputs for all samples. The resampling process then selects a subset of these samples, which we denote $S \subset T$, such that the samples in the subset S follow the desired target density.

Maximum Likelihood Estimation. We learn the inverse warp $z = \Psi_k^{-1}(y)$ using maximum likelihood estimation. Let us assume the warp is parameterized using parameters θ , which we write as $z = \Psi_k^{-1}(y; \theta)$. We first observe that the target density p_Y and the warp Ψ^{-1} are related by the change of variable formula

$$p_Y(y) = \left| \frac{\partial \Psi^{-1}(y; \theta)}{\partial y} \right|. \quad (8)$$

Note that this implies that $z = \Psi_k^{-1}(y)$ is distributed uniformly. The maximum likelihood approach tries to maximize the likelihood that the warp produces the data samples $y_i \sim p_Y$ from uniform samples z_i . More precisely, maximizing the log-likelihood of the data samples $y_i, i \in S$ can be written as

$$\theta^* = \arg \max_{\theta} \sum_{i \in S} \log \left(\left| \frac{\partial \Psi^{-1}(y_i; \theta)}{\partial y_i} \right| \right). \quad (9)$$

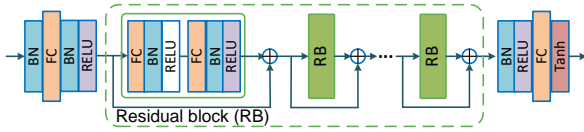


Fig. 5. The neural network architecture to compute the s and t functions in the bijective coupling layers consists of several residual blocks (RB), containing fully connected layers (FC), batch normalization (BN), and ReLU activation units. Additionally, we have fully connected, batch normalization, and activation layers before and after the residual blocks. All fully connected layers contain the same number of neurons.

4.3 PSS Warping using Real NVP

We are leveraging a recent neural network architecture called real-valued non-volume-preserving (Real NVP) transformation [6] to represent and implement our PSS warp Ψ and its inverse. Real NVP has all the desired properties that we need: it is guaranteed to be bijective, it is easy to invert and extend to higher dimensions, the determinant of its Jacobian can be evaluated efficiently, and maximum likelihood estimation can be performed efficiently using gradient descent.

In a nutshell, Real NVP transformations consist of multiple stacked (concatenated) so-called affine coupling layers as shown in Figure 4, top. The mapping computed by each layer is designed to have all the properties mentioned above, and the concatenation of multiple layers can implement complex mappings. Assume each coupling layer computes a mapping from a D -dimensional space onto itself. A key idea is to split the input vector z into two parts, which we represent by a binary mask b of size D . Let $\{b = 1\}$ be the set of indices where the mask has value 1, and similar for $\{b = 0\}$. Each coupling layer forwards the first part of the input $z_{\{b=1\}}$ directly to its output. In addition, the second part of the output $z_{\{b=0\}}$ consists of an affine mapping that is constructed using $s(z_{\{b=1\}})$ and $t(z_{\{b=1\}})$ of the first part of the input. As shown at the bottom left of Figure 4, a coupling layer computes

$$\begin{aligned} z'_{\{b=1\}} &= z_{\{b=1\}} \\ z'_{\{b=0\}} &= z_{\{b=0\}} \odot \exp(s(z_{\{b=1\}})) + t(z_{\{b=1\}}), \end{aligned} \quad (10)$$

where s and t are functions from $\mathbb{R}^{|\{b=1\}|} \rightarrow \mathbb{R}^{|\{b=0\}|}$, and \odot is the element-wise product. Crucially, such a coupling layer is trivial to invert as shown at the bottom right of Figure 4,

$$\begin{aligned} z_{\{b=1\}} &= z'_{\{b=1\}} \\ z_{\{b=0\}} &= (z'_{\{b=0\}} - t(z_{\{b=1\}})) \odot \exp(-s(z_{\{b=1\}})), \end{aligned} \quad (11)$$

and its Jacobian is a triangular matrix whose determinant is also trivial to obtain as $\exp\left(\sum_j s(z_{\{b=1\}})_j\right)$ [6]. Neither operation requires inverting the Jacobians of s and t nor computing their inverses. Hence they can be arbitrarily complex, suggesting their implementation using neural networks. We describe our network architecture to implement s and t in more detail below. Finally, we apply a linear scaling and a logit mapping at the start, and their inverse at the end of the model. We found that this improves training convergence of our model.

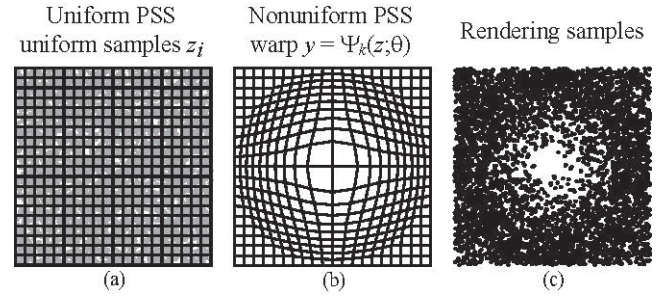


Fig. 6. During rendering, we use the forward warp Ψ to draw an arbitrary number of samples distributed approximately according to the target density. (a) Uniform samples in PSS. (b) Warped PSS using Ψ . (c) Non-uniform samples in PSS, which we provide as input to a black-box renderer.

In summary, we implement our PSS warp Ψ and its inverse using Real NVP with multiple stacked affine coupling layers. Since each bijective coupling layer only warps part of the input dimensions, we concatenate several layers with different masks b to warp all dimensions non-linearly. In our experiments, we always use eight coupling layers and masks where either the even or odd bits are set to zero or one, respectively. We also experimented with other masks, but did not observe any significant differences. The warp parameters θ in Equation 9 correspond to the trainable weights of the neural networks that define the s and t functions in all coupling layers (each layer has its own s and t functions, that is, neural networks). We describe our networks in more detail in the next section. We perform maximum likelihood estimation of Ψ^{-1} using gradient descent and standard backpropagation techniques for neural networks.

4.4 Neural Network Architecture for Coupling Layers

Figure 5 shows the neural network architecture that we use to compute both the s and t functions in Equations 10 and 11. Each function in each coupling layer has its own set of trainable network weights. The network consists of several residual blocks [10], where each block contains two fully connected layers (FC) with batch normalization (BN) and ReLU activations. In addition, there are more such layers before and after the residual blocks. The warping capability of the model is directly affected by the number of coupling layers. More coupling layers enable the model to learn complex mappings. Meanwhile, using more coupling layers and residual blocks will lead to relatively long training time. We discuss the exact network parameters in Section 6.

4.5 Generating Rendering Samples

For rendering, we then use the forward mapping Ψ , which can easily be derived from Ψ^{-1} as shown above. Note that Ψ shares trained parameters of Ψ^{-1} . We generate an arbitrary number of samples distributed approximately according to the target density as represented by the learned warp, as illustrated in Figure 6.

5 APPLICATIONS

While we provide a general framework to learn how to importance sample in primary sample space, we focus on direct and one-bounce

Table 1. Lighting and geometry statistics of our test scenes.

Scene	Triangle count	Light count
Conference	2K	8
Sponza	61.3k	27
Natural history museum	76K	93

indirect illumination in the following experiments. We leave further applications to future work, including effects such as lens sampling, motion blur, or sampling longer paths, which can be naturally included using our framework.

Given any new scene, our method first constructs an initial sample set by shooting a batch of paths using uniform PSS sampling into the scene and computing their contributions. Then we resample this set to obtain samples from the desired target density, which are used as scene-dependent training data in the maximum likelihood estimation (Section 4.2). At run time, the renderer will send uniform random path samples to the trained model, and finally receive warped PSS samples and the corresponding densities (that is, determinants of the Jacobian of the warp), which are then used in the renderer (Section 4.5).

Direct Illumination. Direct illumination computation involves tracing camera rays from the camera to the scene, and estimating outgoing radiance due to incident illumination directly coming from light sources. In our experiments with direct illumination, we warp a three-dimensional PSS vector representing the image plane location of a ray and the light source that is sampled. We do not include the position on the light source in the warp, although this could be useful for scenes with very large area light sources. If multiple importance sampling (MIS) including BSDF sampling is used, there usually are three more random parameters, one for selecting the BSDF component, and the other two for selecting a direction. Since existing BSDF sampling techniques based on analytic expressions generally work well, we currently do not include these parameters in the warp.

One-bounce Indirect Illumination. In addition to direct lighting, we also consider indirect illumination. The light carried by indirect paths generally decreases with an increasing number of path bounces, hence importance sampling one-bounce indirect paths will usually provide the most benefit. In this case, we learn to warp a five dimensional vector consisting of image plane location, indirect bounce direction, and light source index. We do not include MIS similar as in the direct illumination case.

6 EXPERIMENTS AND RESULTS

We implement and train our neural network-based PSS warp using the TensorFlow [1] framework. All experiments are conducted on a workstation with an octa-core 3.60 GHz i7-7700 CPU and Nvidia GeForce GTX 1070 graphics card. The neural network’s computation is implemented on the GPU and the renderer runs on the CPU. Our implementation builds on PBRT [21]. We will release the source code and scene data upon publication of this work.

Our experiments use four test scenes to validate our method. Two of them are variants of the *conference room*, corresponding to two different lighting scenarios. The *conference 1* model contains

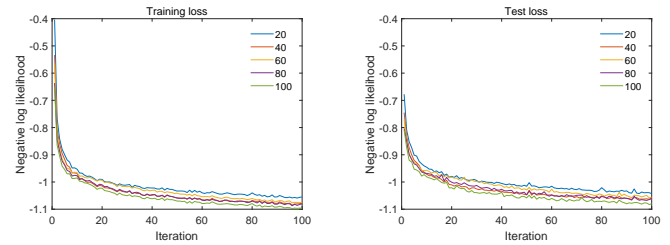


Fig. 7. Comparisons of training and test loss with respect to the number of neurons in the fully connected hidden layers as shown in Figure 5. We use two residual blocks. The training session here runs for up to 100 epochs.

a moderate number of light sources, while *conference 2* contains complex lighting from lights in an adjacent room, where none of the lights are visible to the camera. The *natural history museum* scene contains a large number of light sources. The light source and triangle statistics of each scene are shown in Table 1.

6.1 Model Training and Initialization

For faster convergence during scene-dependent training, we pre-train our neural network to achieve an identity warp. We use the resulting network weights as initialization for scene-dependent training, instead of the usual random initialization. We have observed that this leads to faster scene-dependent training convergence in practice. To get an efficient sampling model, we tend to use lightweight structures with conservative number of coupling layers. We empirically find that using 8 coupling layers is able to learn the target densities in our experiments and keep evaluation cost small. In addition, with a typical network consisting of two residual blocks and forty hidden neurons per fully connected layer (Figure 5), we can compute a gradient descent step for about 16,000 samples per second during training on the Nvidia GeForce GTX 1070 GPU.

6.2 Neural Network Architecture Validation

The capacity of our neural network to represent complex functions is related to the size of the hidden layers (Figure 5). We test several neuron counts per hidden layer ranging from 20 to 100. We use networks with two residual blocks, and train them with the same data. Each training session runs for 100 epochs. Figure 7 presents the training loss and test loss of each network. As can be seen, increasing the number of neurons generally brings lower training and test losses. Meanwhile, using more neurons will form a more complex model, thus leading to longer training time. Accounting for efficiency of training, we use networks with two residual blocks and 40 neurons per hidden layer in our following experiments.

6.3 Training Data Size

In our method, the training data provides an implicit description of the target probability density function. To examine the effects of different numbers of training samples, we train our model with five training data sets of different sizes. We train the model using a low image resolution of 200×160 pixels. Note that the final image can be rendered at an arbitrary, higher resolution. The data set with the smallest scale has 1 sample for each pixel on average. During

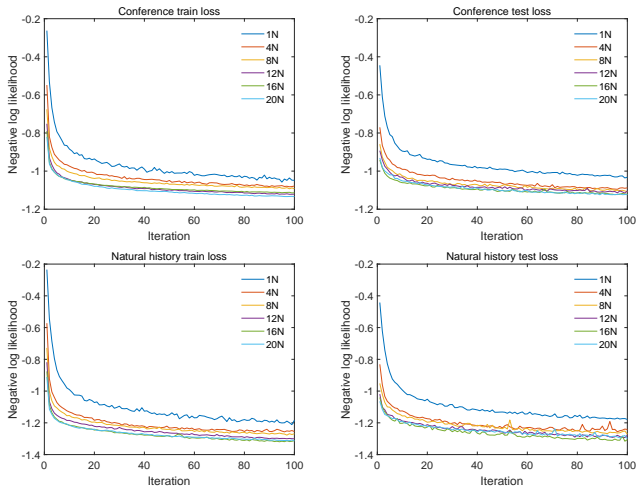


Fig. 8. Comparisons of training loss and test loss with respect to the size of training data sets, plotted over increasing number of training epochs. The training data size is given as a multiple of the training image resolution of 200×160 pixels, indicating how many samples are distributed to a pixel on average. The top row is for the conference scene and the bottom row is for the natural history scene.

training, 80% of the samples are randomly selected as training data and the rest are used for validation purposes. Simultaneously, we provide an accompanying test data set to test the performance of the neural networks. None of the test data are used in the training and validation process.

Figure 8 plots the test loss and training loss for each training data size. It can be observed that a lower negative log likelihood can be obtained with increasing training data size, but the benefits of using more training data quickly vanish after using more than 16spp (samples per pixel), which corresponds to 512,000 samples.

In addition, Figure 9 shows relative L_1 density errors for both training and test data set. The relative density errors can be computed as

$$\epsilon = \frac{1}{N} \sum_{i=1}^N \frac{|P(D_i) - T_i|}{\max(|P(D_i)|, |T_i|)}. \quad (12)$$

Here, $P(D_i)$ stands for the density deduced by the neural network and T_i represents the target density value of D_i . Using more training data helps to reduce relative density errors, but the improvement of density accuracy gets smaller with increasing training data size, and more training data also requires longer training time.

6.4 Convergence Evaluation

Our importance sampling model can be easily applied in the Monte Carlo rendering context, and it helps to reduce variance without introducing bias. This is illustrated in Figure 10, where we compare rendering errors as a function of the average *spp* during rendering, compared to baseline uniform random sampling (i.e., vanilla sampling and rendering without the learned warp). As can be seen, our method provides a consistently lower error and converges without bias. In the *conference 1* scene, our method achieves an average of

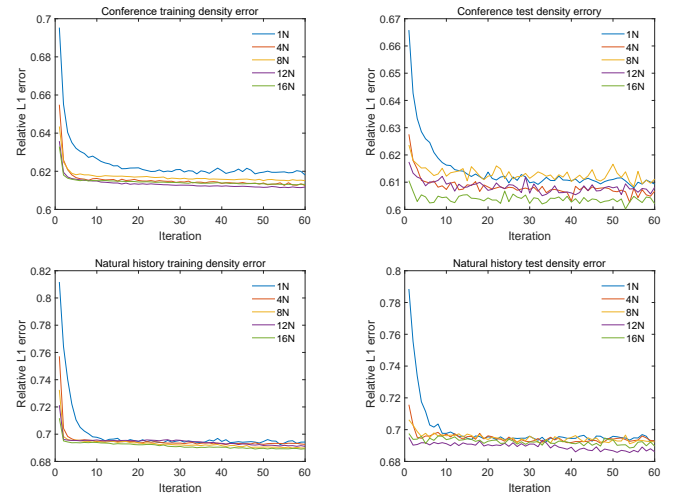


Fig. 9. Relative L_1 density error for training and test data with respect to different scales of training data, indicated as spp at 200×160 resolution.

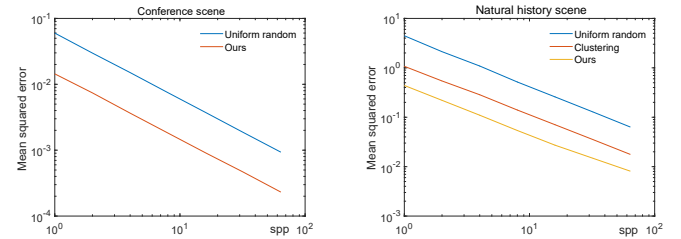


Fig. 10. MSE convergence rates of the conference 1 and natural history scenes. In both cases, our method provides lower errors than the baselines. A logarithmic scale is used on both axes here.

4X acceleration compared to baseline uniform random sampling. For the *natural history* scene, our method utilizes Lightcuts [28] to speed up light sampling. Here, we compare with both the uniform random baseline method and the uniform random method based on Lightcuts. Our method achieves 8.2X and 2.4X faster convergence rates of rendering errors than these two baselines. In addition, it can be observed that our method does not introduce bias and it finally leads to an unbiased Monte Carlo estimator.

To investigate the relationship between rendering errors and the training progress of our neural networks, Figure 11 plots the MSE of images rendered with importance samples produced by the neural networks over the course of training. Each neural network is provided with a training data set of different scale. We find that forty training epochs are typically sufficient to obtain most of the benefit afforded by our method.

6.5 Rendering Results and Further Analysis

Figure 12 shows the rendering results for the three scenes in Table 1. We generally compare with the method of uniformly sampling a light source, sampling based on lights' power, and the method by Donikian et al. [7]. Rendering results of the *conference 1* scene equipped with eight light sources are shown in the first row. Five

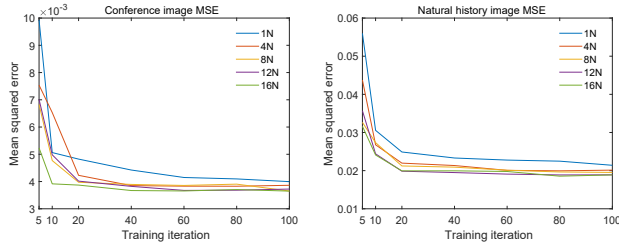


Fig. 11. The relationship between MSE error of rendered images and the number of training epochs of our neural networks, for different sizes of training data as in Figure 9.

light sources with high power are placed in an adjacent room, and they are not visible to the camera. We use eight training samples per pixel, 200×160 training image resolution, and train for forty epochs for our method. Our method is able to learn the distribution of light source contributions, and efficiently distributes samples according to lights' actual contributions. Therefore, given the same rendering time budget, our method provides lower MSE errors than the others. Note that Donikian et al. [7] is slightly sensitive to the parameter selection and there can be some remaining aliasing artifacts.

The second image in Figure 12 shows the Sponza scene, where most of the 27 light sources are not visible to the camera. An other view of the Sponza scene is also shown in Figure 1. We again compare our approach to uniform light sampling, power based light sampling, and Donikian et al. [7]. Similar to the conference scene, we obtain a significant reduction in MSE.

Figure 12 finally shows a natural history museum scene with complex illumination. It contains 92 area lights and one environment light. We use sixteen training samples per pixel, 200×160 training image resolution, and train for forty epochs. The reference image is rendered by a baseline method, which sums up contributions of all light sources for a shading point. It leads to prohibitively long rendering time of 11 hours. To improve rendering efficiency, our method firstly builds a light tree to organize all light sources and we split the scene's space into multiple disjoint regions. Then we compute the lightcut of each region, and select light sources with higher contributions based on the lightcut. We compare our method with the baseline method of uniformly sampling one light, uniform sampling based on lightcuts and Donikian's iterative sampling method. The average percentage of visible lights for a shading point is only 37%. The baseline method is unaware of the visibility difficulty, thus most of its shadow rays are blocked and computation efforts are wasted. Our method is able to learn the shape of the manifold of light path samples in the primary sample space and generates new samples on the manifold. Therefore, lower errors can be achieved.

In Figure 13 we visualize the image space distribution of samples generated by our neural networks and compare it with the distribution of ground truth image brightness. Our method effectively detects regions with high luminance and intelligently places more samples there. In addition, this example demonstrates again that our neural importance sampling model can robustly learn the designated sampling density and generate new samples from the target distribution.

Figure 14 of *conference 2* demonstrates a typical lighting challenge. Light sources are not directly visible to the camera and most visible areas from the camera receive only indirect illumination coming from the adjacent room. We therefore use this setup to evaluate our approach with 1-bounce indirect illumination and a five-dimensional warp as described in Section 5. Specifically, we will learn the distribution of 1-bounce indirect paths and importance sample the distribution to generate new paths samples, such that the rendering errors are minimized. Here, we collect eight samples per pixel at 200×160 image resolution for training data, and the training session runs for 25 epochs. We compare our method with the baseline method of both equal samples and equal rendering time, excluding training time. We do not include Donikian et al.'s method here, since it is specifically designed for direct illumination computation. Due to the importance samples obtained from the primary sample space, our method performs better than others both in visual quality and in numerical errors.

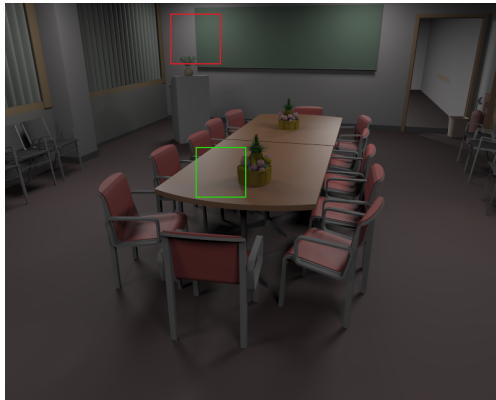
7 DISCUSSION AND LIMITATIONS

A downside of our approach is that it requires a training phase that takes on the order of a few minutes in general. In addition, the accuracy of the density produced by our warp depends on the amount of training data, and using more training data increases training time. While Real NVP supports warps with thousands of dimensions [6], we have experimented with up to five dimensions and a few hundred thousand training samples so far. Higher-dimensional warps may be challenging to learn in practice because of the required amount of training samples. Our framework could also be applied in different variants, however, for example by learning multiple lower-dimensional, local warps on different slices of path space in a flexible manner, instead of one global one.

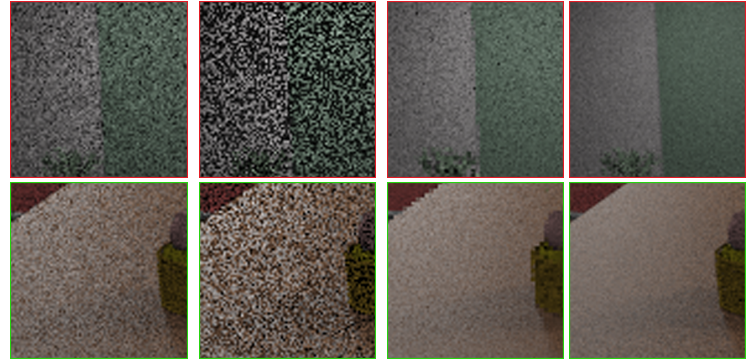
Our current approach is most beneficial when the training effort can be amortized over time consuming rendering of high quality, high resolution output images. Evaluating the PSS warp to generate samples during rendering also includes some overhead, but this is typically only a small percentage of the cost of acquiring each path sample. In our experiments, the variance reduction afforded by the warp far outweighs its runtime costs as shown in Figure 14 for example. Finally, unlike other methods that learn local, directional sampling densities in an a posteriori manner [19, 27], our method is agnostic of the underlying light transport effect and can also be applied to lens or temporal sampling, and participating media.

8 CONCLUSIONS AND FUTURE WORK

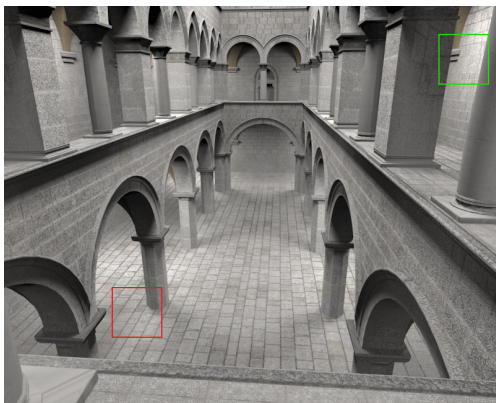
We have introduced a novel approach to learn importance sampling of entire light paths in primary sample space using a suitable neural network architecture. We leverage the neural network to perform a non-linear warp in primary sample space, achieving a desired target density that can further reduce the variance of an existing renderer, which is treated as a black box by our method. Our experiments show that this approach can effectively reduce variance in practical scenarios without introducing bias. A main advantage of our approach is that it is agnostic of specific light transport effects in any scene, and the underlying renderer. Therefore, it is easy to



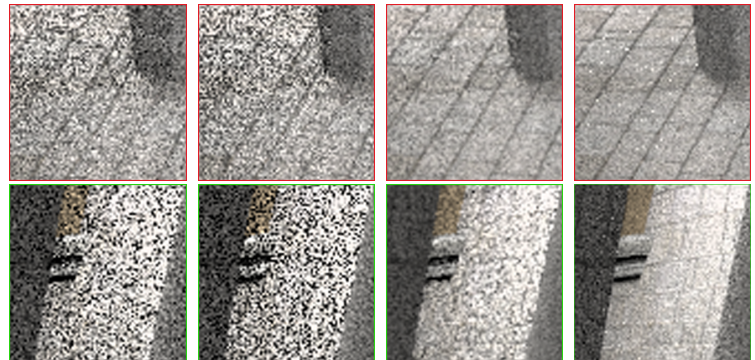
Conference room reference, 8 lights



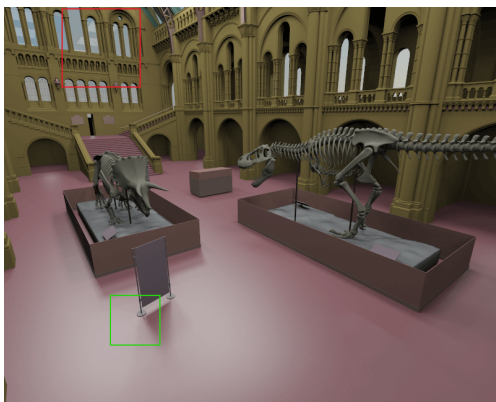
Uniform random	Power based sampling	Donikian et al.	Ours
0.00189138	0.00878227	0.00117945	0.000438677



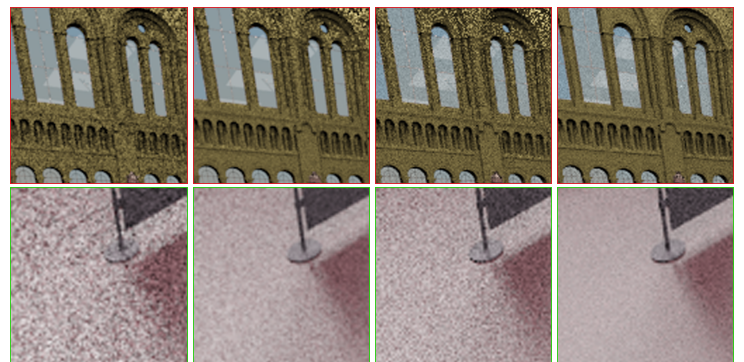
Sponza reference, 27 lights



Uniform random	Power based sampling	Donikian et al.	Ours
0.0279182	0.0240422	0.0091250	0.00607132



Natural history museum reference, 93 lights



Uniform random	Donikian et al.	Clustering	Ours
0.065283	0.0330481	0.0176721	0.010391

Fig. 12. Visual comparison of our method for direct illumination rendering with uniform random sampling one light, power based light sampling, Donikian et al. [7], and cluster based sampling. The MSE numbers show that our method achieves a significant error reduction compared to the baselines.

implement it on top of existing systems. In the future we will evaluate our approach using higher dimensional warps for longer light paths, and including additional effects such as depth of field, motion blur, and participating media. An other interesting avenue for future research is to extend our maximum likelihood approach to a

Bayesian framework with a prior, which could allow more effective scene-dependent training using fewer samples.

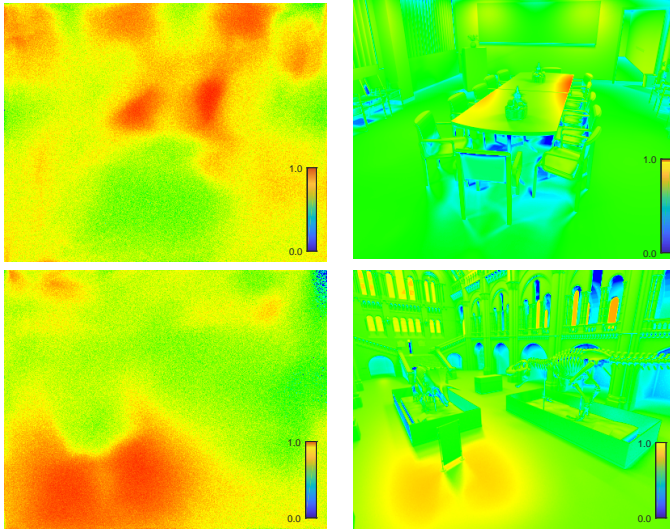


Fig. 13. Comparison of image space sample distribution (left column) and ground truth image luminance distribution (right column). The top row is the conference 1 scene and the bottom row is for the natural history scene.

REFERENCES

- [1] Martin Abadi, Ashish Agarwal, Paul Barham, Eugene Brevdo, Zhifeng Chen, Craig Citro, Greg S. Corrado, Andy Davis, Jeffrey Dean, Matthieu Devin, Sanjay Ghemawat, Ian Goodfellow, Andrew Harp, Geoffrey Irving, Michael Isard, Yangqing Jia, Rafal Jozefowicz, Lukasz Kaiser, Manjunath Kudlur, Josh Levenberg, Dandelion Mané, Rajat Monga, Sherry Moore, Derek Murray, Chris Olah, Mike Schuster, Jonathon Shlens, Benoit Steiner, Ilya Sutskever, Kunal Talwar, Paul Tucker, Vincent Vanhoucke, Vijay Vasudevan, Fernanda Viégas, Oriol Vinyals, Pete Warden, Martin Wattenberg, Martin Wicke, Yuan Yu, and Xiaoqiang Zheng. 2015. TensorFlow: Large-Scale Machine Learning on Heterogeneous Systems. (2015). <https://www.tensorflow.org/> Software available from tensorflow.org.
- [2] Steve Bako, Thijs Vogels, Brian McWilliams, Mark Meyer, Jan Novák, Alex Harvill, Pradeep Sen, Tony DeRose, and Fabrice Rousselle. 2017. Kernel-predicting Convolutional Networks for Denoising Monte Carlo Renderings. *ACM Trans. Graph.* 36, 4, Article 97 (July 2017), 14 pages. <https://doi.org/10.1145/3072959.3073708>
- [3] Benedikt Bitterli, Wenzel Jakob, Jan Novák, and Wojciech Jarosz. 2017. Reversible jump metropolis light transport using inverse mappings. *ACM Transactions on Graphics (TOG)* 37, 1 (2017), 1.
- [4] Chakravarty Reddy Alla Chaitanya, Anton Kaplanyan, Christoph Schied, Marco Salvi, Aaron Lefohn, Derek Nowrouzezahrai, and Timo Aila. 2017. Interactive Reconstruction of Monte Carlo Image Sequences using a Recurrent Denoising Autoencoder. *ACM Transactions on Graphics* (Aug 2017).
- [5] Petrik Clarberg, Wojciech Jarosz, Tomas Akenine-Möller, and Henrik Wann Jensen. 2005. Wavelet Importance Sampling: Efficiently Evaluating Products of Complex Functions. *ACM Trans. Graph.* 24, 3 (July 2005), 1166–1175. <https://doi.org/10.1145/1073204.1073328>
- [6] Laurent Dinh, Jascha Sohl-Dickstein, and Samy Bengio. 2016. Density estimation using Real NVP. *CoRR* abs/1605.08803 (2016).
- [7] M. Donikian, B. Walter, Kavita Bala, S. Fernandez, and D. P. Greenberg. 2006. Accurate direct illumination using iterative adaptive sampling. *IEEE Transactions on Visualization and Computer Graphics* 12, 3 (May 2006), 353–364. <https://doi.org/10.1109/TVCG.2006.41>
- [8] Ian Goodfellow, Jean Pouget-Abadie, Mehdi Mirza, Bing Xu, David Warde-Farley, Sherjil Ozair, Aaron Courville, and Yoshua Bengio. 2014. Generative Adversarial Nets. In *Advances in Neural Information Processing Systems 27*, Z. Ghahramani, M. Welling, C. Cortes, N. D. Lawrence, and K. Q. Weinberger (Eds.). Curran Associates, Inc., 2672–2680. <http://papers.nips.cc/paper/5423-generative-adversarial-nets.pdf>
- [9] Toshiya Hachisuka, Anton S Kaplanyan, and Carsten Dachsbacher. 2014. Multiplexed metropolis light transport. *ACM Transactions on Graphics (TOG)* 33, 4 (2014), 100.
- [10] K. He, X. Zhang, S. Ren, and J. Sun. 2016. Deep Residual Learning for Image Recognition. In *2016 IEEE Conference on Computer Vision and Pattern Recognition*

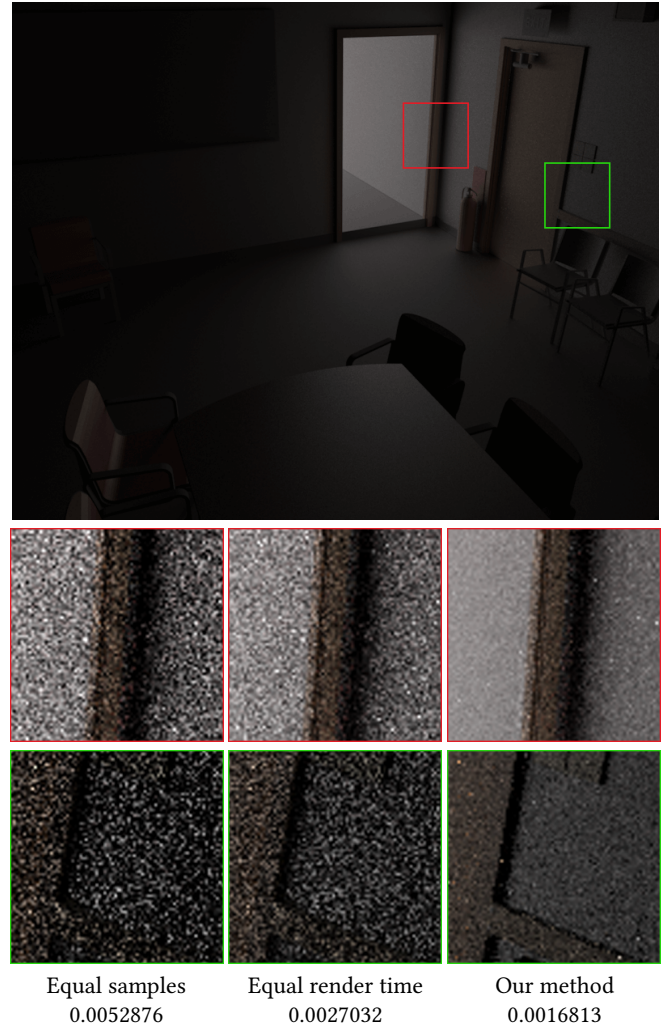


Fig. 14. Challenging lighting scenario rendered with one bounce indirect illumination. We use a five dimensional warp in our method, representing the image space location, indirect bounce direction, and light source selection. The left and middle columns use a baseline solution with BRDF importance sampling for the indirect bounce, and uniform sampling for light selection. The rendering time for our method on the right is 127s with 32 rendering samples per pixel. We show equal rendering time and equal spp to allow fair comparison of MSE numbers. The reference image at the top is rendered by the baseline method for 2 hours.

- (CVPR), 770–778. <https://doi.org/10.1109/CVPR.2016.90>
- [11] Eric Heitz and Eugene d'Eon. 2014. Importance Sampling Microfacet-Based BSDFs using the Distribution of Visible Normals. *Computer Graphics Forum* 33, 4 (2014), 103–112.
- [12] Wenzel Jakob and Steve Marschner. 2012. Manifold exploration: a Markov Chain Monte Carlo technique for rendering scenes with difficult specular transport. *ACM Transactions on Graphics (TOG)* 31, 4 (2012), 58.
- [13] James T Kajiya. 1986. The rendering equation. In *ACM Siggraph Computer Graphics*, Vol. 20. ACM, 143–150.
- [14] Simon Kallweit, Thomas Müller, Brian McWilliams, Markus Gross, and Jan Novák. 2017. Deep Scattering: Rendering Atmospheric Clouds with Radiance-predicting Neural Networks. *ACM Trans. Graph.* 36, 6, Article 231 (Nov. 2017), 11 pages. <https://doi.org/10.1145/3130800.3130880>

- [15] Anton S Kaplanyan, Johannes Hanika, and Carsten Dachsbacher. 2014. The natural-constraint representation of the path space for efficient light transport simulation. *ACM Transactions on Graphics (TOG)* 33, 4 (2014), 102.
- [16] Csaba Kelemen, László Szirmay-Kalos, György Antal, and Ferenc Csonka. 2002. A simple and robust mutation strategy for the metropolis light transport algorithm. In *Computer Graphics Forum*, Vol. 21. Wiley Online Library, 531–540.
- [17] Diederik P. Kingma and Max Welling. 2014. Auto-Encoding Variational Bayes. In *ICLR*.
- [18] Tzu-Mao Li, Jaakko Lehtinen, Ravi Ramamoorthi, Wenzel Jakob, and Frédo Durand. 2015. Anisotropic gaussian mutations for metropolis light transport through hessian-hamiltonian dynamics. *ACM Transactions on Graphics (TOG)* 34, 6 (2015), 209.
- [19] Thomas Müller, Markus Gross, and Jan Novák. 2017. Practical Path Guiding for Efficient Light-Transport Simulation. In *Computer Graphics Forum*, Vol. 36. Wiley Online Library, 91–100.
- [20] Hisanari Otsu, Anton S Kaplanyan, Johannes Hanika, Carsten Dachsbacher, and Toshiya Hachisuka. 2017. Fusing state spaces for markov chain monte carlo rendering. *ACM Transactions on Graphics (TOG)* 36, 4 (2017), 74.
- [21] Matt Pharr, Wenzel Jakob, and Greg Humphreys. 2016. *Physically Based Rendering: From Theory to Implementation* (3 ed.). Morgan Kaufmann.
- [22] Peiran Ren, Jiaping Wang, Minmin Gong, Stephen Lin, Xin Tong, and Baining Guo. 2013. Global Illumination with Radiance Regression Functions. *ACM Trans. Graph.* 32, 4, Article 130 (July 2013), 12 pages. <https://doi.org/10.1145/2461912.2462009>
- [23] Justin F. Talbot, David Cline, and Parris Egbert. 2005. Importance Resampling for Global Illumination. In *Proceedings of the Sixteenth Eurographics Conference on Rendering Techniques (EGSR '05)*. Eurographics Association, Aire-la-Ville, Switzerland, Switzerland, 139–146. <https://doi.org/10.2312/EGWR/EGSR05/139-146>
- [24] Eric Veach and Leonidas J Guibas. 1995. Optimally combining sampling techniques for Monte Carlo rendering. In *Proceedings of the 22nd annual conference on Computer graphics and interactive techniques*. ACM, 419–428.
- [25] Eric Veach and Leonidas J Guibas. 1997. Metropolis light transport. In *Proceedings of the 24th annual conference on Computer graphics and interactive techniques*. ACM Press/Addison-Wesley Publishing Co., 65–76.
- [26] Petr Věvoda, Ivo Kondapaneni, and Jaroslav Krivánek. 2018. Bayesian online regression for adaptive direct illumination sampling. *ACM Transactions on Graphics (Proceedings of SIGGRAPH 2018)* 37, 4 (2018).
- [27] Jiří Vorba, Ondřej Karlík, Martin Šik, Tobias Ritschel, and Jaroslav Krivánek. 2014. On-line learning of parametric mixture models for light transport simulation. *ACM Transactions on Graphics (TOG)* 33, 4 (2014), 101.
- [28] Bruce Walter, Sebastian Fernandez, Adam Arbree, Kavita Bala, Michael Donikian, and Donald P. Greenberg. 2005. Lightcuts: A Scalable Approach to Illumination. *ACM Trans. Graph.* 24, 3 (July 2005), 1098–1107. <https://doi.org/10.1145/1073204.1073318>